HIPPOCAMPUS 18:1239–1255 (2008)

Conversion of a Phase- to a Rate-Coded Position Signal by a Three-Stage Model of Theta Cells, Grid Cells, and Place Cells

Hugh T. Blair,[1]* Kishan Gupta,[1] and Kechen Zhang[2]

ABSTRACT: As a rat navigates through a familiar environment, its position in space is encoded by firing rates of place cells and grid cells. Oscillatory interference models propose that this positional firing rate code is derived from a phase code, which stores the rat's position as a pattern of phase angles between velocity-modulated theta oscillations. Here we describe a three-stage network model, which formalizes the computational steps that are necessary for converting phase-coded position signals (represented by theta oscillations) into rate-coded position signals (represented by grid cells and place cells). The first stage of the model proposes that the phase-coded position signal is stored and updated by a bank of ring attractors, like those that have previously been hypothesized to perform angular path integration in the head-direction cell system. We show analytically how ring attractors can serve as central pattern generators for producing velocity-modulated theta oscillations, and we propose that such ring attractors may reside in subcortical areas where hippocampal theta rhythm is known to originate. In the second stage of the model, grid fields are formed by oscillatory interference between theta cells residing in different (but not the same) ring attractors. The model's third stage assumes that hippocampal neurons generate Gaussian place fields by computing weighted sums of inputs from a basis set of many grid fields. Here we show that under this assumption, the spatial frequency spectrum of the Gaussian place field defines the vertex spacings of grid cells that must provide input to the place cell. This analysis generates a testable prediction that grid cells with large vertex spacings should send projections to the entire hippocampus, whereas grid cells with smaller vertex spacings may project more selectively to the dorsal hippocampus, where place fields are smallest. © **2008 Wiley-Liss, Inc.**

KEY WORDS: hippocampus; entorhinal cortex; ring attractor; oscillatory interference; head-direction cells

INTRODUCTION

Animals can maintain an internal representation of their own spatial position as they navigate through the world (Tolman, 1948). This involves a process of path integration, whereby the animal keeps track of its position by integrating the velocity of its own navigational movements over time. Following the discovery that the rodent hippocampus contains place cells which fire selectively at preferred locations (O'Keefe and Dostrovsky, 1971), it was theorized that the hippocampus might contain a neural circuit for path integration (O'Keefe and Nadel, 1978; Touretzky and Redish, 1996; Redish and Touretzky, 1997; Samsonovich and McNaughton, 1997). However, it was subsequently discovered that place cells receive input from grid cells in the entorhinal cortex, which exhibit a different kind of spatial tuning: each grid cell sketches a periodic hexagonal lattice across the surface of the rat's environment (Hafting et al., 2005; Moser and Moser, 2008). The discovery of grid cells has fueled speculation that the primary circuit for path integration may reside in the entorhinal cortex (Hafting et al., 2005; Fuhs and Touretzky, 2006; McNaughton et al., 2006). Here, we argue that path integration of translational movements may not occur in the hippocampus or entorhinal cortex, but is instead performed by subcortical central pattern generators (CPGs) that generate velocity-modulated theta oscillations.

Our reasoning for this argument is based upon a computational theory called the "oscillatory interference model" (O'Keefe and Recce, 1993; Burgess et al., 2005, 2007; O'Keefe and Burgess, 2005), which proposes an elegant principle to explain how grid cells derive their spatially periodic firing patterns. This model posits that grid cells convert a phase-coded signal of the rat's position (represented by theta oscillations) into a firing rate-coded signal (represented by grid cells and place cells). Before this conversion, the rat's position is encoded by the relative phases of multiple theta oscillators, rather than by the firing rates of individual neurons. Oscillatory interference models imply that the neural substrate for storing the phase-coded position signal may be the same as that for generating theta oscillations. Here, we propose that theta rhythm is produced by subcortical ring attractor networks that function as frequency-modulated oscillators, and that these networks provide the neural substrate for storing and updating the phase-coded position signal. This hypothesis is consistent with existing evidence that theta rhythm originates within the subcortical structures where we postulate that the ring attractors are located (Vertes and Kocsis, 1997; Vertes et al., 2001; Pan and McNaughton, 2004; Sharp and Koester, 2008).

In accordance with the principles of oscillatory interference, we show that outputs from theta cells residing in different (but not the same) ring attractors can be combined to form spatially periodic oscillations, which are similar to the observed firing patterns of grid cells. Hence, grid cells can form their spatially periodic firing fields by summing inputs from

[1] **Psychology Department, University of California, Los Angeles, California;** [2] **Department of Biomedical Engineering, Johns Hopkins University School of Medicine, Baltimore, Maryland**

Grant sponsor: NIH; Grant number: R01MH079511 [NSF Collaborative Research in Computational Neuroscience (CRCNS)].

*Correspondence to: Hugh T. Blair, UCLA Psychology Department, 1285 Franz Hall, Los Angeles, CA 90095-1563, USA. E-mail: blair@psych.ucla.edu

Accepted for publication 27 August 2008
DOI 10.1002/hipo.20509
Published online 19 November 2008 in Wiley InterScience (www.interscience.wiley.com).

different subcortical ring oscillators. Grid cells in entorhinal cortex send projections to place cells in the hippocampus, which are thought to form unitary firing fields by combining inputs from multiple grid cells (O'Keefe and Burgess, 2005; McNaughton et al., 2006; Rolls et al., 2006; Solstad et al., 2006; Fiete et al., 2008; Hayman and Jeffery, 2008; Molter and Yamaguchi, 2008). We have previously shown that place cells can form unitary Gaussian firing fields by linearly summing inputs from multiple grid cells (Blair et al., 2007). Here we demonstrate that when a Gaussian place field is formed in this way, the weight vector of synaptic connections from grid cells onto the place cell is analogous to the spatial frequency spectrum of the Gaussian place field. Consequently, the place cell must sum inputs from grid cells that cover the entire range of spatial frequencies within the spectrum of the Gaussian place field. All Gaussian place fields (large or small) contain power at the lowest spatial frequencies, but only small place fields contain power at higher spatial frequencies. This leads to the prediction that place cells cannot exhibit unitary firing fields of any size (large or small) in large environments unless they integrate inputs from grid cells with large vertex spacings; however, only place cells with small firing fields require input from grid cells with small vertex spacings. Since place fields grow larger along the septo-temporal axis of the hippocampus (Jung et al., 1994; Maurer et al., 2005; Kjelstrup et al., 2008), and grid fields grow larger (hence, spatial frequencies grow smaller) along the dorsoventral axis of the entorhinal cortex (Hafting et al., 2005; Sargolini et al., 2006; Brun et al., 2008), our spatial frequency analysis of place fields leads to specific predictions about the pattern of anatomical projections from entorhinal grid cells to hippocampal place cells. We present simulations to suggest how these theoretical predictions can be experimentally tested.

OSCILLATORY INTERFERENCE MODELS OF PATH INTEGRATION

Oscillatory interference models of spatial path integration are descended from "dual oscillator models" that were originally proposed to explain the phenomenon of theta phase precession in hippocampal place cells (O'Keefe and Recce, 1993; O'Keefe and Burgess, 2005). As a moving rat enters a place cell's firing field, the cell begins to fire action potentials in characteristic bursts referred to as "complex spikes" (Fig. 1). Each complex spike burst is a barrage of action potentials that occurs within the time window of a single theta cycle period (about 150 ms). O'Keefe and Recce (1993) discovered that as a rat runs through the preferred firing field of a place cell, the timing of complex bursts emitted by the place cell exhibits a stereotyped phase relationship with theta oscillations in the locally recorded EEG signal.

Phase Precession by Hippocampal Place Cells

Consider a rat running in one direction along a linear track, as shown at the top of Figure 1. If the rat enters a place cell's firing field (gray shaded area), the place cell will start firing in complex bursts. Since the rat first enters the place field at its periphery (where the mean firing rate of the place cell is low), there will be relatively few spikes generated during the first complex burst. O'Keefe and Recce (1993) discovered that this first complex burst is also likely to occur just prior to the valley of the locally recorded theta EEG signal (red sinusoid at the bottom of Fig. 1). Under the convention that the valley of the theta EEG signal corresponds to zero degrees of phase, this means that the place cell fires late in the phase of the theta rhythm as the rat first enters the cell's place field. The place cell then falls silent for a period of time that is, on average, slightly less than one cycle period of the theta oscillation, and then a second complex spike burst is initiated. The second burst is likely to contain more spikes than the first, since the rat moves closer to the center of the cell's place field (where the cell's mean firing rate is higher) between the first and second complex bursts. And since the interval period between complex spike bursts is a bit less than the period of one theta cycle, the second complex burst is initiated at a slightly earlier phase of the theta EEG signal than the first. Consequently, the place cell's complex bursts exhibit "phase precession" with respect to the locally recorded theta EEG signal (bottom of Fig. 1).

The Dual Oscillator Model of Phase Precession

To account for the phase precession phenomenon, O'Keefe and Recce (1993) proposed that place cells may be driven by a second oscillatory input (green sinusoid in Fig. 1) that has a slightly higher frequency—and thus a slightly shorter period—than the theta EEG frequency. This would explain why the interval between a place cell's complex bursts is slightly shorter than the interval between cycles of the theta EEG rhythm, thereby producing the phase precession effect.

When two oscillators with slightly differing frequency (detuned oscillators) are combined, they gradually move in and out of phase with each other, alternately interfering constructively and destructively to produce an "envelope" waveform (blue trace in Fig. 1). The interference waveform has two distinct frequency components: a high-frequency "carrier" component and a low-frequency "beat" component. The carrier frequency is equal to the mean of the two detuned oscillator frequencies:

$$f_i^C = \frac{f_0 + f_i}{2}, \tag{1}$$

where f_i^C denotes the carrier frequency produced by a pair of detuned oscillators with frequencies f_0 and f_i. The beat frequency is equal to the absolute value of the difference between the frequencies of the detuned oscillators:

$$f_i^B = |f_0 - f_i|. \tag{2}$$

Figure 1 illustrates how the dual oscillator model can explain phase precession as a rat runs on a linear track at a fixed speed of 30 cm/s. In this example, a place cell is driven by two detuned theta oscillators with frequencies of $f_0 = 7$ Hz (red

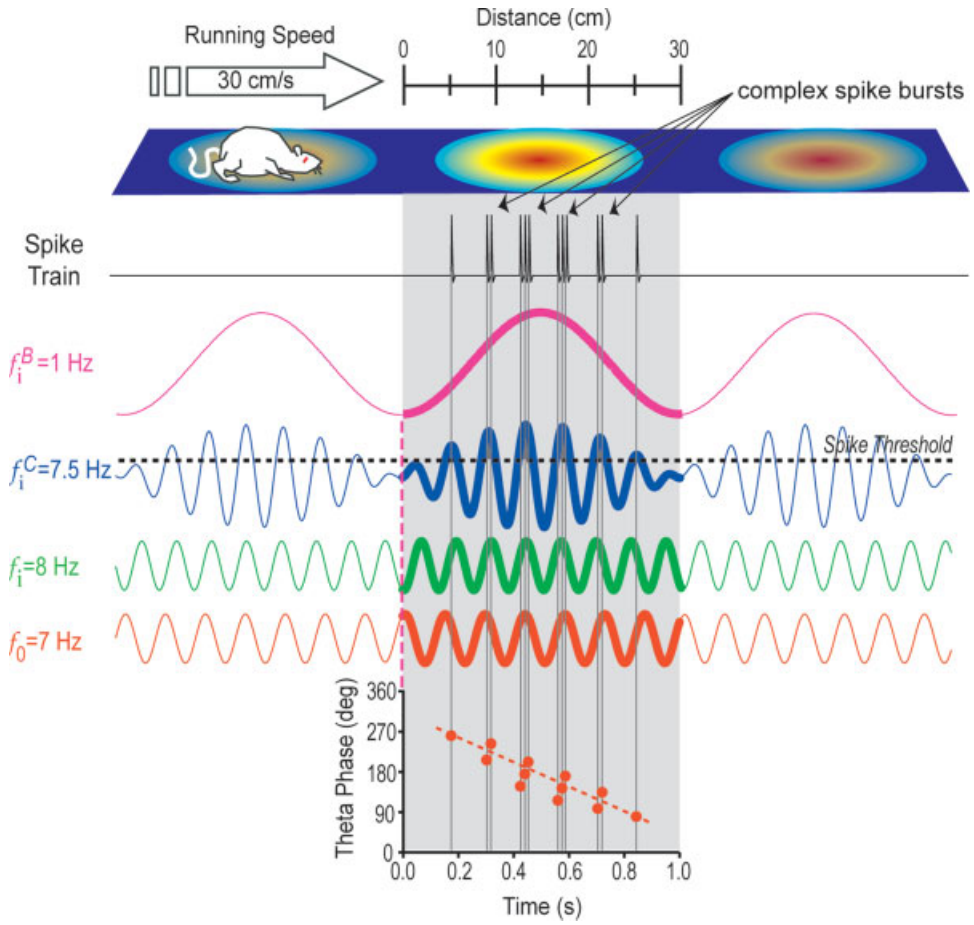

FIGURE 1. Producing grid fields by beat interference between theta oscillators. As a rat runs across a linear track at a constant speed of 30 cm/s (top), a pair of detuned theta oscillators with frequencies of 7 Hz (red) and 8 Hz (green) interfere with each other to produce a 1-Hz beat oscillation (magenta) riding on a 7.5-Hz carrier (blue). If the blue trace is assumed to be a place or grid cell's membrane potential, then the cell will fire when its membrane potential exceeds a spike threshold (dashed line). Spikes come in bursts (black lines) at the 7.5-Hz carrier frequency, and undergo phase precession against the 7-Hz theta oscillator (bottom graph). [Color figure can be viewed in the online issue which is available at www.interscience.wiley.com.]

trace) and f_i = 8 Hz (green trace). This produces an interference waveform with a carrier frequency of $f_i^C = 7.5$ Hz (blue trace) and a beat frequency of $f_i^B = |7 - 8| = 1$ Hz (magenta trace). We assume that the blue trace corresponds to the membrane potential of a hippocampal place cell, and the cell's spike threshold (dashed line in Fig. 1) is set so that spiking occurs only when the membrane potential exceeds the spike threshold. Under these assumptions, the place cell fires only at the peaks of the carrier cycles during the constructive interference phase (but not the destructive interference phase) of the beat cycle. Each crossing of the spike threshold by the place cell membrane potential produces a burst of spikes, and the number of spikes in each burst is proportional to the area of the interference waveform above threshold on each carrier cycle. Consequently, there are more spikes per burst at the peak of the beat cycle (in the center of the place field) than off the peak of the beat cycle (at the periphery of the place field). Moreover, the timing of the threshold crossings (and therefore, of spikes emitted by the place cell) on successive carrier cycles precesses through the phase of the f_0 oscillator, just as place cell spikes precess through the phase of the hippocampal EEG (Fig. 1, bottom). Hence, this dual oscillator model can account for phase precession (O'Keefe and Recce, 1993).

If place fields are formed by beat interference between detuned oscillators, then why don't place cells exhibit slow, rhythmic "beating" at the frequency f_i^B, as predicted by Eq. (2)? In other words, why does each place cell tend to fire only in one location of an environment, rather than firing over and over again at regular time intervals as detuned theta inputs move in and out of phase with the beat cycle? O'Keefe and Burgess (2005) recognized that the discovery of grid cells in entorhinal cortex might hold an answer to this puzzling question; place cells do not exhibit oscillatory firing at low frequencies, but grid cells do (Hafting et al., 2005; Moser and Moser, 2008).

Oscillatory Interference Models of Grid Cells

As a rat runs through an open-field environment, a grid cell fires action potentials at multiple vertex points that are geomet-

rically arranged to form a hexagonal lattice pattern—or grid field—which tessellates across the surface of the environment (Hafting et al., 2005). When a rat runs along a straight linear track, the two-dimensional structure of the grid field collapses into one dimension, forming a periodic series of vertex bumps at evenly spaced intervals along the track, similar to the evenly spaced peaks of the beat cycle in Figure 1. In this one-dimensional rendering of the grid field, we may define the vertex spacing λ as the distance between adjacent bumps (i.e., the beat wavelength). For simplicity, we shall consider only the one-dimensional case of grid fields on a linear track in the present study. Other models have addressed how the oscillatory interference principle can be extended to simulate two-dimensional grid fields (Burgess et al., 2005, 2007; Blair et al., 2007; Giocomo et al., 2007; Hasselmo et al., 2007; Burgess, 2008; Hasselmo, 2008), and extension of the one-dimensional network implementation proposed here into two dimensions will be considered in the discussion.

We have seen that a 1-Hz beat oscillation can be produced when theta oscillators of 7 and 8 Hz interfere with one another (Fig. 1). If a rat is running at a constant speed of 30 cm/s, then the peaks of this 1 Hz beat pattern will occur exactly 30-cm apart (once per second), emulating fluctuations in the mean firing rate of a grid cell with $\lambda = 30$ cm. In the rat brain, grid cell vertex spacings vary over a range from about 30 cm up to several meters (Hafting et al., 2005; Sargolini et al., 2006; Brun et al., 2008). To simulate grid cells with different vertex spacings, we may vary the frequency of the beat oscillation (O'Keefe and Burgess, 2005; Blair et al., 2007; Giocomo et al., 2007; Giocomo and Hasselmo, 2008). A beat oscillation with frequency f_i^B (produced from theta frequencies f_0 and f_i) can emulate a grid cell with an arbitrary vertex spacing, λ_i, given by the formula

$$\lambda_i = \frac{v}{f_i^B} = \frac{v}{|f_0 - f_i|}, \tag{3}$$

where v denotes the rat's running speed, which is taken to be non-negative ($v \geq 0$). Equation (3) states that the vertex spacing of a grid cell not only depends upon the beat frequency, f_i^B, but also upon the rat's running speed, v (because the faster the rat is running, the farther it travels on each beat cycle, and larger the vertex spacing, λ_i). This is problematic, because real grid cells exhibit the same vertex spacing for all running speeds, and thus λ_i should not depend upon v as stated by Eq. (3). The problem here is that the dual oscillator model generates beat oscillations that repeat themselves over fixed intervals of time, whereas grid cells produce firing rate patterns that repeat themselves over fixed intervals of space. Consequently, the dual oscillator model can only simulate grid cells for the special case when a rat is running at a constant velocity (when the beat oscillations have both a constant spatial and temporal frequency). How can the model be modified to produce grid fields that have a constant spatial frequency (rather than a constant temporal frequency) at all running speeds?

An elegant solution to this problem was first demonstrated by Burgess et al. (2005), and subsequently implemented in later models (Blair et al., 2007; Burgess et al., 2007; Giocomo et al., 2007; Hasselmo et al., 2007; Giocomo and Hasselmo, 2008). The solution is to make the beat frequency f_i^B inversely proportional to the rat's running speed, so that when the rat speeds up or slows down, the numerator and denominator of Eq. (3) change by inverse proportions to maintain a fixed spatial period for the beat oscillation, λ_i. For the case of a rat running on a linear track, this occurs when

$$f_i^B = \frac{v}{\lambda_i}, \tag{4}$$

where λ_i is a constant that defines the fixed (nonvelocity-dependent) spatial period of the beat oscillation (and hence the vertex spacing of the grid field). In Eq. (4), we see that the frequency of the beat oscillation now increases in proportion with the rat's running speed, v; this makes sense, because each cycle of the beat oscillation corresponds to a single traversal of a grid vertex, and if successive vertices are spaced at a fixed distance (λ_i) apart from each other, they will be encountered more frequently as the rat runs faster. We can also see from Eq. (4) that the slope (or gain) of f_i^B's velocity dependence is inversely proportional to the vertex spacing parameter, λ_i; this also makes sense, because the closer the grid vertices are to one another (i.e., the smaller λ_i is), the more frequently they will be encountered at any given running speed.

Equations (2) and (4) provide complementary expressions for the beat frequency, f_i^B. By Eq. (2), f_i^B is the absolute value of the difference between theta frequencies f_0 and f_i. Combining the two is equivalent to Eq. (3), which can be rewritten as

$$f_i = f_0 \pm \frac{v}{\lambda_i}. \tag{5}$$

In conjunction with the arguments presented above, Eq. (5) implies that if two theta frequencies, f_0 and f_i, are "detuned" in linear proportion with the rat's running speed, v, and the slope of this linear relationship is $1/\lambda_i$, then the two theta oscillators will interfere with one another to produce a beat oscillation whose frequency, f_i^B, is variable over fixed intervals of time but constant over fixed intervals of space, with a spatial period equal to λ_i. Hence, the beat cycle will emulate the spatially periodic firing pattern of a grid cell with vertex spacing λ_i on a linear track.

The relationship between v and f_i^B becomes more complicated in open-field environments, where grid fields exhibit hexagonal geometry, because in this case, the spacing between grid bumps depends upon the direction as well as the speed of movement. To simulate the hexagonal structure of grid fields in a two-dimensional environment, Eqs. (4) and (5) can be modified by introducing a directional vector component for the velocity term, v (Burgess et al., 2007; Giocomo et al., 2007; Hasselmo et al., 2007; Burgess, 2008). An alternative solution is to assume that f_0 and f_i denote the frequencies of two-dimensional theta oscillators, or "theta grids" (Blair et al., 2007). Here, we disregard these complexities by considering only the case of the rat running on a linear track; extension to the open field is addressed in the Discussion.

Grid Cells Convert a Phase Code Into a Rate Code of the Rat's Position

We have seen that if two theta oscillators obey the relation specified in Eq. (5), then they will interfere with one another to produce a beat oscillation with a fixed spatial period, λ_i. This means that as a rat runs on a linear track, the amplitude of the beat oscillation will be identical at every position $x \pm k\lambda_i$ on the track (where k is an arbitrary integer). The beat amplitude will thus behave like the mean firing rate of a grid cell with vertex spacing λ_i (see Fig. 1).

Since the beat cycle is produced by interference between a pair of theta oscillators, its amplitude is determined by the phase difference between these two oscillators. Hence, the amplitude of the interference pattern at position x may be expressed as

$$B_i(x) = \left[2A\left|\cos\frac{\phi_0 - \phi_i}{2}\right| - C\right]_+, \qquad (6)$$

where ϕ_0 and ϕ_i denote the phases of each of the two theta oscillators, whose amplitude is given by A, and C is spike threshold (see Fig. 1). The brackets indicate rectification, with $[x]_+ = x$ for $x > 0$, and 0 otherwise. The left-hand side of Eq. (6) denotes an amplitude signal, which can be equated with the firing rate of a grid cell at a position x on a linear track. The right-hand side of Eq. (6) denotes a phase angle between two theta oscillators, which is identical at all positions $x \pm k\lambda_i$ on the track. Note that x does not appear on the right side of Eq. (6), because the rat's position is encoded by the phase difference $\phi_0 - \phi_i$, and not by ϕ_0 or ϕ_i alone (both oscillators can assume any phase at any position; it is only the phase difference—and not the absolute phase—which is constrained by position).

Equation (6) tells us that in oscillatory interference models, grid cells convert a phase code of the rat's position [right side of Eq. (6)] into a firing rate code [left side of Eq. (6)]. The position signal originates within the phase differences between the theta oscillators, which is in turn derived by velocity-dependent modulation of theta oscillator frequencies [Eq. (5)]. Consequently, the neural substrate for the phase-coded position signal is the same as the substrate for generating velocity-modulated theta rhythm. So if we wish to know how the phase-coded position signal is produced, we must consider how theta rhythm is generated.

GENERATING VELOCITY-MODULATED THETA RHYTHM

According to the oscillatory interference model, accurate path integration requires the frequencies of theta oscillators to be very precisely modulated by the rat's movement velocity [Eq. (5)]. Moreover, since phase angles between different theta oscillators encode the rat's position [Eq. (6)], the oscillators must maintain stable phase relationships with one another over behaviorally relevant time scales (many seconds, or dozens of theta cycle periods). Hence, oscillatory interference models impose strict constraints upon the dynamical properties of theta oscillators. It is not presently known whether these constraints are satisfied by theta-generating circuits in the rat brain, and if so, how. To address this question, we must ask where theta rhythm comes from; theta oscillations can be generated at the level of individual neurons by intracellular membrane oscillations, or at the network level by reverberatory circuits consisting of multiple neurons (Buzsaki, 2002; Acker et al., 2003; Lengyel et al., 2003; Giocomo et al., 2007; Hasselmo et al., 2007; Giocomo and Hasselmo, 2008).

Subthreshold Membrane Oscillations

Intrinsic membrane currents can generate intracellular theta oscillations in place cells and grid cells, and it has been hypothesized that these intrinsic oscillations may combine with one another to produce phase precession and beat interference patterns that underlie positional coding (Lengyel et al., 2003; Burgess et al., 2007; Hasselmo et al., 2007; Giocomo and Hasselmo, 2008). Interestingly, there is a strong correlation between the spatial frequency of grid cell firing patterns and the temporal frequency of subthreshold membrane oscillations at different positions along the dorsoventral axis of the entorhinal cortex (Giocomo et al., 2007; Giocomo and Hasselmo, 2008). Based on this evidence, it has been suggested that subthreshold membrane oscillations within grid cells could play a role in generating the theta oscillations from which grid cell firing patterns are derived, and thereby, contribute to their spatial tuning properties.

But can intrinsic membrane oscillations by themselves (without external synchronization) be stable enough to store accurate phase information across many theta cycle periods, as required for accurate positional coding in oscillatory interference models? Internal membrane oscillations are produced by voltage-sensitive currents, and consequently, perturbations of a neuron's membrane potential can easily upset the phases of such oscillations. Large voltage perturbations—such as those that occur during action potentials—can instantaneously reset the phases of subthreshold oscillations throughout a neuron. Grid cells can fire several spikes per theta cycle when the rat visits a grid vertex, so if the spatially periodic firing patterns of a grid cell arise from oscillatory interference between membrane fluctuations within the grid cell itself, how can the position signal survive erasure by the grid cell's own action potentials?

Instead of generating velocity-modulated theta oscillations, subthreshold membrane currents may serve a different, but equally important function: by determining the resonant frequencies of grid cell dendrites, oscillatory membrane currents could control the AC impedances of those dendrites at different oscillation frequencies. Inputs from external oscillators that match the dendrite's resonant frequency would have a larger effect on the postsynaptic membrane potential than other inputs. So, the resonant frequency of a grid cell's dendrite

could determine which external oscillatory inputs best excite the grid cell, which would be critical for determining the spatial tuning properties of the grid cell, in agreement with the elegant experiments of Giocomo et al. (2007). But, where might external oscillatory inputs to grid cells come from? Hasselmo (2008) has proposed that such inputs might come from nearby entorhinal pyramidal neurons, which can fire persistently at very stable frequencies (Egorov et al., 2002). Here, we propose an alternative possibility: grid cells may receive external oscillatory inputs from subcortical ring attractor circuits that generate velocity-modulated theta rhythm.

Subcortical Networks for Generating Theta Rhythm

In the mammalian nervous system, many of the CPG circuits that control rhythmic motor behaviors are found along the rostrocaudal axis of the brainstem and spinal cord. Evidence suggests that movement-related hippocampal theta rhythm (Vanderwolf, 1969) originates from subcortical circuits in the midbrain and mammillary bodies, which are positioned near the rostral pole of this axis (Vertes and Kocsis, 1997; Vertes et al., 2001; Pan and McNaughton, 2004). Here, we propose that these subcortical areas may contain CPG circuits for producing velocity-modulated theta oscillations, and thereby provide the neural substrate for storing and updating the phase-coded position signal. We hypothesize that the theta CPG circuit may be functionally similar to the rodent head-direction circuit, which monitors the directional position of the rat's head by integrating the angular velocity of head turning movements over time. Since the head-direction circuit is an angular path integrator, it performs a function very similar to that of translational path integrator described by oscillatory interference models; the primary difference is that the head-direction circuit integrates an angular velocity signal, whereas the oscillatory interference circuit integrates a translational velocity signal. We will demonstrate below that both types of path integration can be performed by similar ring attractor networks. Before explaining this further, it is useful to briefly review the principles underlying ring attractor models of the head-direction system.

Ring Attractor Models of the Head-Direction Circuit

Head-direction cells encode a rat's directional heading in the horizontal (yaw) plane; each head-direction cell is tuned to fire selectively when the animal faces in its preferred direction (north, southwest, etc.), and remains silent when the rat is facing other directions (Taube et al., 1990). The population of head-direction cells is thought to serve as a "mental compass," which underlies the rat's internal sense of direction (Taube et al., 1990; Skaggs et al., 1995). Directional heading is a variable which assumes values that lie upon a circle (like a compass), so we may think of the rat's directional heading as the "phase angle" between the rat's head and the static surrounding environment. Theoretical models of the head-direction circuit have hypothesized that the directional signal may be generated by a ring attractor network (Fig. 2A), a circular layer of neurons in which adjacent head-direction cells encode similar headings (Skaggs et al., 1995; Redish et al., 1996; Zhang, 1996a,b; Song and Wang, 2005). A rat can only face in one direction at a time, so activity in the network must always be localized to a small group of adjacent neurons with similar directional preferences, to encode the direction the rat is currently facing. If nonadjacent neurons were concurrently active in the network, then this would imply that the rat was facing in multiple directions at once, which is impossible. Hence, the only stable "attractor states" of the head-direction circuit should be those in which a localized "bump" of persistent activity is located at a position on the ring that corresponds to the rat's current directional heading.

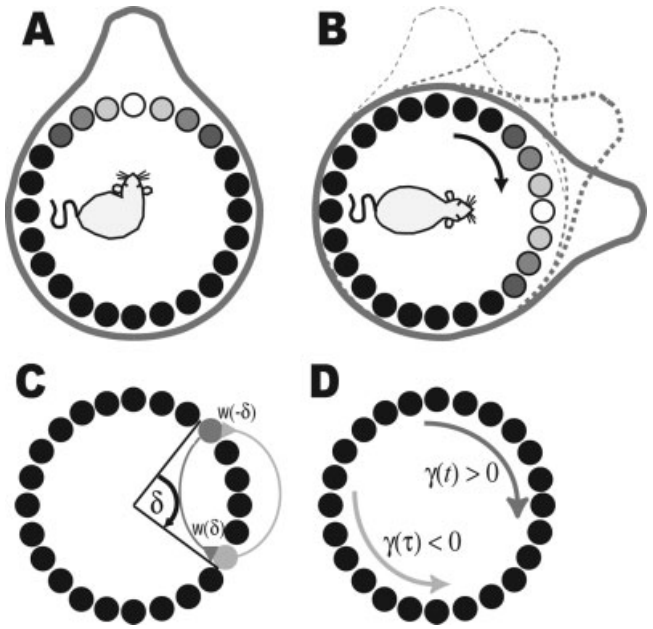

FIGURE 2. Ring attractor model of the rat head-direction circuit. (A) A stationary activity bump when the head is still. (B) A shifting bump when the rat is turning. (C) Reciprocal weights in the ring attractor. (D) Direction and speed of an oscillating bump depend upon the weighting coefficient, $\gamma(t)$, for the asymmetric weight component [Eq. (9)].

The persistent activity bump should be able to rest at any position on the ring to encode any direction the rat might face. Hence, the ring attractor has many "neutrally stable" attractor states in which the activity bump can rest at any position on the ring (analogous to a ball which can rest stably at any location on a flat tabletop). The stability of the persistent activity bump depends sensitively upon the pattern of connections between neurons in the ring. To sustain a localized activity bump, the connection pattern must satisfy two major constraints. First, the connections between neurons in the network should be rotation-invariant, meaning that the strength of the connection between any two neurons depends only upon how far apart they are from one another on the ring (or equivalently, upon the angular difference between their directional

tuning preferences), and not upon their individual directional tuning preferences. Second, the connections should implement a center-surround pattern of excitation and inhibition, so that neurons which are near each other (and thus have similar directional preferences) exert an excitatory influence upon one another, and neurons that are distant from each other (and thus have dissimilar directional preferences) exert an inhibitory influence upon one another. For appropriate parameter values satisfying these constraints, the network can exhibit stable attractor states in which a small group of neighboring neurons remain active by mutually exciting one another, while all of the other neurons within the ring are silenced by surrounding inhibition from the active subpopulation, forming a stable activity bump at an arbitrary position on the ring.

When the rat is not turning its head (and therefore facing in a constant direction), the activity bump should remain stationary at a fixed position on the ring. This occurs when the connections between neurons are symmetrical, so that

$$w(\delta) = w(-\delta), \tag{7}$$

where w denotes the connection strength between any pair of neurons with directional tuning preferences that differ by the angle δ (Fig. 2C). Equation (7) states that the strength of the connection between two neurons in the ring does not depend upon the sign of the difference between their tuning preferences, so the connection from neuron i to neuron j has the same strength as the connection from j to i. To satisfy the center-surround constraint, we additionally assume that w is positive (an excitatory connection) if $|\delta|$ is small (neurons are near to one another on the ring), and w is negative (an inhibitory connection) if $|\delta|$ is large (neurons are far from one another on the ring).

The rat's directional heading changes whenever it turns its head, and this requires new head-direction cells to become active while previously active cells fall silent. This can be achieved if the activity bump shifts dynamically around the ring as the rat turns its head. An example of this is illustrated in Figure 2B; a rat begins by facing north (so the activity bump in the ring attractor is centered over cells that encode north), then turns clockwise to face east. The activity bump shifts clockwise around the ring as the rat turns, until the bump is centered over cells that prefer east. How can the activity bump shift through the ring in this way? We have already seen that when the pattern of connections among the neurons is symmetrical, the bump remains stationary at a single position on the circle. To shift the bump around the ring, the symmetry of the connection pattern can be adjusted so that cells excite or inhibit their neighbors on one side more than the other. In other words, the symmetry expressed by Eq. (7) is broken, and

$$w(\delta) \neq w(-\delta). \tag{8}$$

This asymmetry of the connection pattern can cause the bump to propagate around the ring toward the direction of greater excitation, or conversely, away from the direction of greater inhibition. Here, we adopt the convention that excitation is greater in the clockwise direction (and inhibition is greater in the counterclockwise direction) when $w(\delta) > w(-\delta)$, and that the reverse is true when $w(\delta) < w(-\delta)$. In the example of Figure 2B, as the rat turns from facing north to east, we assume that $w(\delta) > w(-\delta)$ during the clockwise head turn, so that the activity bump shifts clockwise around the ring from north to east. When the rat stops turning its head, the symmetry of the connections is restored, and the bump rests at a new stable position over cells that encode east.

The Spatial Derivative Law and Its Implementation by Coupled Networks

A potential problem with the shifting process that occurs under asymmetric weights [Eq. (8)] is that changing the attractor network's connections can destroy the stability of the activity bump. The propagating activity bump can retain a stable shape that is identical to the stationary shape only when the connections in the network obey a "spatial derivative law," which means that the strength of the connection between two neurons on the ring can be subdivided into two terms as follows:

$$w(\delta, t) = W(\delta) + \gamma(t) W'(\delta). \tag{9}$$

Notice that the connection between the pair of cells now depends not only upon the difference between their preferred directions, δ, but also upon time (denoted by t). This reflects the fact that the connection strength will differ from one moment to the next, depending upon the rat's head-turning behavior. Changes in the connection strength are governed by a time-varying coefficient, $\gamma(t)$, which is proportional to the angular velocity of the rat's head at time t. At times when $\gamma(t) = 0$ (i.e., when the rat is not turning its head), Eq. (9) becomes $w(\delta) = W(\delta)$. Therefore, assuming that $W(\delta)$ is a symmetrical, center-surround connection pattern that satisfies the relation in Eq. (7), then the activity bump will remain stationary at a fixed location on the ring when the rat's head is not turning. But when $\gamma(t) \neq 0$, Eq. (9) states that an asymmetric component $W'(\delta)$ is added into the weight vector. In this case, cells no longer excite and inhibit each other equally in both directions. As shown in Figure 2D, the bump will shift in the clockwise direction when $\gamma(t) > 0$ and, in the counterclockwise direction when $\gamma(t) > 0$.

Zhang (1996a) has proved that the activity bump will retain its shape during the shifting state only if $W'(\delta)$ is proportional to the spatial derivative of $W(\delta)$. A biologically plausible network architecture for enforcing this spatial derivative rule can be implemented by coupling two ring attractor with asymmetric weights that are proportional to the spatial derivative (Zhang, 1996a,b). As shown by various models (Xie et al., 2002; Song and Wang, 2005), modifying the driving inputs to the coupled rings can bias their competition in a manner that

is equivalent to adding time-varying asymmetric weights as in Eq. (9). If these driving inputs are proportional to angular head velocity, it is possible for an activity bump representing the rat's directional heading to shift through the ring attractor network without losing its shape as the rat turns its head.

The Ring Attractor As a Frequency-Modulated Oscillator

The ring attractor model of head-direction cells has two dynamical states: a static state in which the activity bump remains stationary on the ring (when the head is not turning), and a dynamic state in which the activity bump circulates around the ring (when the head is turning). The static state prevails when the network's connection pattern is symmetric [Eq. (7)], and the dynamic state prevails when asymmetry is introduced into the connection pattern by angular velocity signals [Eq. (9)].

This ring attractor model of angular path integration by head-direction cells can easily be modified to create an oscillator, simply by assuming that the tonic "ground state" of the network is the dynamic state (a shifting activity bump at constant speed), rather than the static state (a stationary activity bump). To implement this assumption, we may specify that excitation and inhibition in the network obey the spatial derivative rule and are asymmetric [$\gamma(t) \neq 0$ in Eq. (9)] by default, at all times. In this case, the activity bump should retain its shape while circulating around the ring attractor at an instantaneous angular speed given by

$$\omega(t) = -\frac{\gamma(t)}{\tau}, \tag{10}$$

where $\omega(t)$ is the angular speed (in radians/s) of the activity bump at time t, $\gamma(t)$ is the weighting coefficient for the asymmetric component of the ring attractor's connection pattern at time t [from Eq. (9)], and τ is a time constant governing how fast the individual neurons in the ring attractor can change their activity. The instantaneous frequency (in Hz) at which the activity bump circulates around the ring is equal to

$$f(t) = \frac{\omega(t)}{2\pi}. \tag{11}$$

We can see from Eq. (11) that if the activity bump's angular speed lies on the interval $8\pi < \omega < 24\pi$ (per second), then the bump will circulate around the ring at a frequency within the theta band of 4–12 Hz. Hence, the ring attractor network can function as a CPG for generating theta rhythm. Since the exact frequency of CPG oscillation depends upon the asymmetric weighting coefficient $\gamma(t)$, it is possible to introduce linear velocity dependence of the theta oscillation's frequency by specifying that

$$\gamma(t) = \Lambda_0 + Hv(t), \tag{12}$$

where $v(t)$ is the rat's movement velocity at time t, H is a constant that determines the gain of velocity modulation, and Λ_0 is a constant bias term that determines the baseline oscillation frequency when the rat is not moving (i.e., when $v = 0$).

The only difference between a ring attractor model for angular path integration by head-direction cells vs. translational path integration by theta oscillators is how we choose to assign value to the variables in Eq. (12). To obtain a model of head-direction cells, we take $v(t)$ to be the angular velocity of the head, and set $\Lambda_0 = 0$ so that the ground state of the network is a stationary activity bump when the head is not turning. To obtain a CPG for producing velocity-modulated theta rhythm, we take $v(t)$ to be the translational velocity of the rat, and set $8\pi\tau < \Lambda_0 < 24\pi\tau$ so that the ground state of the network is a circulating activity bump that generates theta-frequency oscillations. As the activity bump circulates around the ring of the theta CPG, each neuron in the network bursts rhythmically at the frequency $f(t)$ given by Eq. (11), and each burst is centered upon a phase given by

$$\phi_j = \frac{2\pi j}{N}, \tag{13}$$

where ϕ_j denotes the bursting phase for the j^{th} neuron in the ring, and N denotes the total number of neurons in the ring. Hence, the "receptive field" of each neuron in the ring is not a directional heading, but a particular phase of the CPG's oscillation (a phase code). In the next section, we show that such phase coding by individual neurons is extremely useful for constructing "topographic maps" of grid cells in the entorhinal cortex to support spatial path integration.

A THREE-STAGE NETWORK MODEL

In this section, we describe a three-stage network model to demonstrate how a phase-coded position signal represented by theta cells can be transformed into a periodic firing rate code represented by grid cells on a one-dimensional linear track, and then into an aperiodic firing rate code represented by place cells (Fig. 3). It is shown that when place fields are modeled as Gaussians produced by linear summation of grid fields (Blair et al., 2007), the spatial frequency spectrum of the Gaussian determines the vertex spacings of grid fields that must be summed to produce the place field.

Layer I: Theta Cells

Figure 3 shows that our model's first stage is a bank of "ring attractors" for generating velocity-modulated theta rhythm, as described above. Each neuron in the first stage is a theta cell residing within one of these ring attractors. A useful characteristic of this arrangement is that it provides an architecture for "sorting" theta oscillations according to their frequency and phase; theta cells residing within different rings oscillate at different frequencies, whereas theta cells residing within the same ring oscillate at different phases of the same frequency. In simulations presented here, we used 13 rings (or frequencies) consisting of 6 cells (or phases) per ring, so there were $13 \times 6 =$

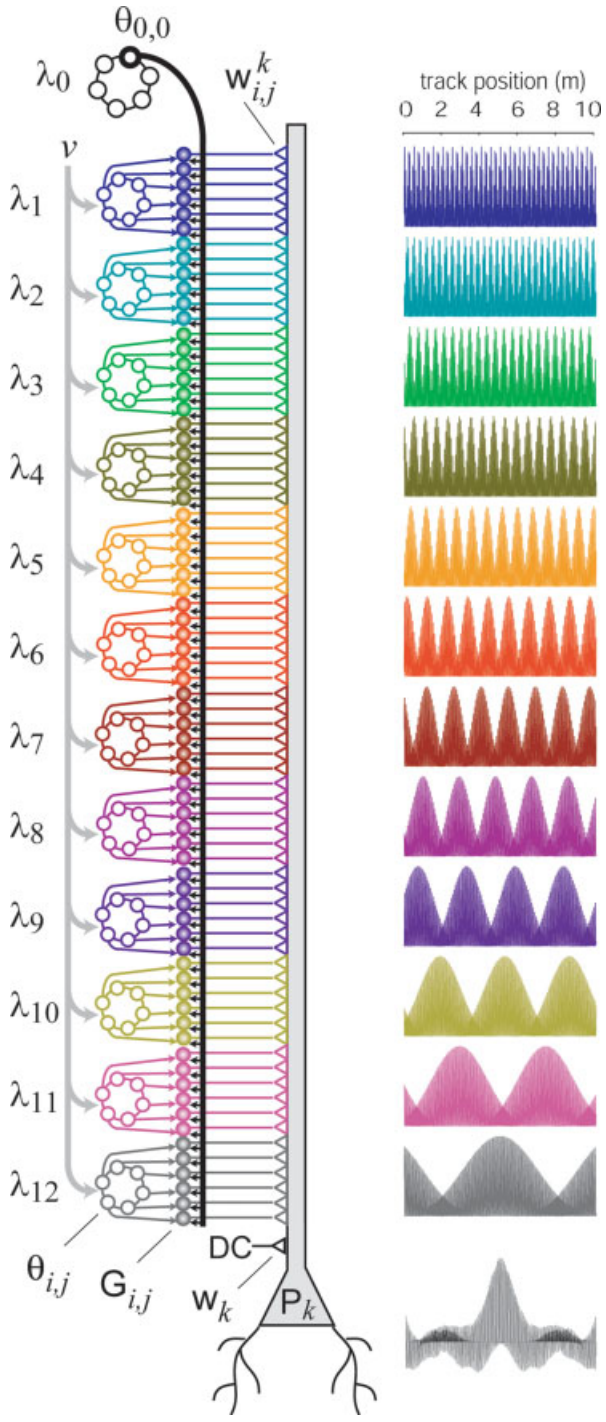

FIGURE 3. A three-stage model of theta cells, grid cells, and place cells. The model's first stage is a bank of ring attractors consisting of theta cells; λ_0 denotes a "reference ring" oscillating at a frequency that does not depend on velocity; $\lambda_1, \ldots, \lambda_{12}$ are "theta rings" oscillating at frequencies modulated by velocity with differing gains. Each grid cell in the second stage receives a shared input from theta cell $\theta_{0,0}$ in the reference ring, and an unshared input from a cell $\theta_{i,j}$ in one of the theta rings. The place cell in the third stage sums weighted inputs from grid cells to produce a Gaussian place field. [Color figure can be viewed in the online issue which is available at www.interscience.wiley.com.]

78 theta cells in the first stage of the model. For computational efficiency, we did not simulate the network dynamics of the ring attractors. Instead, the activity levels of theta cells were simulated as sinusoids with amplitudes that ranged between 0 and 1 at time-varying frequencies. This was done at each simulation time step t by assigning

$$\theta_{i,j}(t) = \frac{\sin\left(\alpha_i(t) + \phi_j\right) + 1}{2}, \tag{14}$$

where $\theta_{i,j}(t)$ is the activation of j^{th} theta cell in the i^{th} ring, ϕ_j is a phase offset for the j^{th} theta cell in every ring [from Eq. (13)], and $\alpha_i(t) = 2\pi \int_0^t f_i(T)dT$ is the phase of the i^{th} ring at time t, with $f_i(T)$ being the oscillation frequency of the i^{th} ring. We may regard $\theta_{i,j}$ as a matrix of sinusoids in which frequencies (theta rings) are indexed by i and phases (theta cells) are indexed by j.

The value of $f_i(T)$ at each time step was computed using Eq. (5), with $f_0 = 7$ Hz as the "reference frequency." By Eq. (5), $f_i(T)$ exceeded the reference frequency of 7 Hz by an amount proportional to the running speed $v(t)$ of the simulated rat, and inversely proportional to a gain factor λ_i that was different for each theta ring. We set $\lambda_0 = 0$ for the first ring (indexed by $i = 0$), so that it became a "reference oscillator" with a constant frequency of 7 Hz, regardless of running speed. The other 12 rings (indexed by $1 \leq i \leq 12$) were assigned gain parameters so that when paired with the 7 Hz reference oscillator, they would produce grid spacings that were evenly distributed on a logarithmic axis between a minimum of $\lambda_1 = 25$ cm and a maximum of $\lambda_{12} = 600$ cm (see Fig. 3, right column).

Layer II: One-Dimensional Grid Cells

The model's second stage was a matrix of one-dimensional grid cells, each of which fired at evenly spaced intervals along a linear track (see left side of Fig. 3). Each of the one-dimensional grid cells received two inputs: one from the theta cell at phase position $j = 0$ in the reference oscillator (henceforth denoted as $\theta_{0,0}$), and another from an arbitrary theta cell $\theta_{i,j}$ in one of the other 12 theta rings. Since all grid cells received shared input from $\theta_{0,0}$, the only thing that distinguished one grid cell from another was the identity of its second unshared input, $\theta_{i,j}$. The first stage of the model contained 12 rings other than the reference oscillator, each consisting of 6 theta cells, so that there were $12 \times 6 = 72$ unique grid cells in the network. The activation of grid cell $G_{i,j}$ at time t was computed as the product of its two theta cell inputs,

$$G_{i,j}(t) = \theta_{0,0}(t) \times \theta_{i,j}(t). \tag{15}$$

We have taken the product of the theta oscillations rather than the sum, because the sum is a linear transformation whereas the product is nonlinear, and the nonlinearity was necessary for reasons explained later (see below, "Nonlinearity requirement"). Elsewhere in this issue, Burgess (2008) shows

that grid fields produced by additive vs. multiplicative interference share similar spatial tuning properties.

The frequency of the shared theta input $\theta_{0,0}$ was fixed at the reference frequency of $f_0 = 7$ Hz, regardless of the rat's running speed. By contrast, the frequency $f_i(t)$ of the unshared theta input $\theta_{i,j}$ varied with the rat's running speed by an amount that depended upon the gain parameter, λ_i, for the i^{th} ring that $\theta_{i,j}$ resided in. Consequently, the output of grid cell $G_{i,j}$ was an interference pattern with two distinct frequency components: a carrier frequency f_i^C given by Eq. (1), and a beat frequency f_i^B given by Eqs. (2) and (5). The beat frequency f_i^B had a fixed spatial period, λ_i, which determined the vertex spacing of grid cell $G_{i,j}$. Hence, the vertex spacing of each grid cell, $G_{i,j}$, was equal to the λ_i parameter of the theta cell, $\theta_{i,j}(t)$, that provided the unshared input to that grid cell. This means that all grid cells receiving their unshared input from the same ring i had the same vertex spacing, λ_i; but their grid fields were not identical because the translational phase of the grid field depended upon the phase (indexed by j) of the grid cell's unshared theta input.

Layer III: Place Cells

The model's third stage was a layer of place cells, each receiving weighted inputs from all 72 one-dimensional grid cells. The activation of the k^{th} place cell at time t was

$$P_k(t) = w_k + \sum_{i=1}^{M-1} \sum_{j=0}^{N-1} w_{i,j}^k G_{i,j}(t), \quad (16)$$

where $w_{i,j}^k$ is the weighting coefficient for the place cell's input from grid cell $G_{i,j}$, and w_k is a constant term that can be regarded the weight of a DC input, which represents a grid cell with infinitely large vertex spacing. The preferred firing location of place cell k was chosen by assigning weights $[w_k, w_{1,1}^k, w1_{1,2}^k, w_{1,3}^k, \ldots, w_{M,N}^k]$ to its inputs from grid cells, $G_{i,j}$. As in Blair et al. (2007), we used the Moore–Penrose pseudoinverse method to assign weighting coefficients so that the place field P_k would optimally fit a Gaussian target function representing a single location on a simulated linear track, given by

$$V_k(x) = -70 + D \exp\left(-\frac{(x-\mu)^2}{2\sigma^2}\right), \quad (17)$$

where $V_k(x)$ is the desired DC membrane potential (in mV) of place cell P_k at position x (in cm) on the track, σ is the standard deviation (in cm) of the target Gaussian place field, μ is the center location of the place field on the track, and $D - 70$ is membrane potential at the peak position while -70 is the resting potential far away from the peak. Since Eq. (17) defines a place cell's mean membrane voltage at each position on the track, the fitted output of our simulated place cells, P_k, was also expressed as a membrane voltage [Eq. (16)]. Equation (16) approximates Eq. (17) as a linear sum of periodic grid functions (including an input with infinite period, weighted by w_k).

Spatial Frequency Spectrum of a Gaussian Place Field

Equation (16) models a Gaussian place field [defined by Eq. (17)] as a linear weighted sum of periodic grid fields with different spatial frequencies. Thus, the weight vector $[w_k, w_{1,1}^k, w1_{1,2}^k, w_{1,3}^k, \ldots, w_{M,N}^k]$ is analogous to the spatial frequency spectrum of the Gaussian place field. From linear systems theory, the spectrum of the Gaussian, $V_k(x)$, is another Gaussian in the domain of spatial frequencies

$$F(\omega) = \left| \int_{-\infty}^{\infty} (V_k(x) + 70) \exp(-i\omega x) dx \right| = \sqrt{2\pi}\sigma D \exp\left(-\frac{\omega^2}{2\sigma^{-2}}\right), \quad (18)$$

where $F(\omega)$ is the amplitude of the place field's spectrum at spatial frequency ω, and D is the peak value of the Gaussian from Eq. (17). If we wish to construct a Gaussian place field as a linear sum of grid fields, Eq. (18) tells us what range of spatial frequencies must be contained in the grid field basis set to get a good fit, and how each frequency should be weighted. The main factor that determines these spatial frequencies is the size of the Gaussian place field, which is governed by the width parameter, σ. Note that the vertex spacing (or spatial wavelength) of a grid field, λ, is the inverse of its spatial frequency, so $\lambda = 1/\omega$. Place cells increase their field size along the septo-temporal axis of the hippocampus (Jung et al., 1994; Maurer et al., 2005; Kjelstrup et al., 2008), and grid cells decrease their spatial frequencies along the dorsoventral axis of the entorhinal cortex (Hafting et al., 2005; Sargolini et al., 2006; Brun et al., 2008). In simulations below, it is shown that Eq. (18) can constrain which grid cells should project to place cells along the septo-temporal axis of the hippocampus.

Nonlinearity Requirement

Our three-stage model (Fig. 3) converts a phase-coded position signal represented by theta cells into a periodic rate-coded position signal represented by grid cells, and then into an aperiodic rate-coded position signal represented by place cells. Grid cells perform an essential intermediate step in this conversion process, because no linear combination of theta oscillations can generate a Gaussian place field. There are two reasons for this. First, place fields have a center and width that is fixed in space, but theta oscillations have variable spatial frequencies and phases that depend upon the rat's running velocity. Second, even in the special case of constant running velocity (where theta oscillations have fixed spatial frequencies and phases), the spatial frequencies of theta oscillations are narrowly distributed within a range that does not cover the spectrum of Gaussian place fields. For example, if a rat runs at a constant speed of 50 cm/s, the spatial period of a 7-Hz theta oscillation would be $\sim$7 cm. This lies at the upper boundary of the spatial frequency spectrum for the smallest place fields in the dorsal hip-

pocampus, and is completely outside the spectrum for larger place fields in ventral hippocampus (see Fig. 5D below). Consequently, theta oscillations are useless as basis functions for constructing Gaussian place fields by linear summation.

Although a Gaussian place field cannot be created by linearly combining theta oscillations, it can be created by linearly combining grid fields, because grid fields possess both the critical properties that the theta oscillations lack: fixed spatial beat periods and phases at all running speeds, and low spatial frequencies that lie within the spectrum of hippocampal place fields. But grid fields are "spawned" from theta oscillations, so how is creating place cells out of grid cells different from creating place cells out of theta oscillations? The answer is that the system that converts theta oscillations into grid fields must incorporate a nonlinear transformation, because if it does not, the system reduces to a linear model in which we are trying to construct Gaussian place fields as a weighted sum of theta oscillations, which is impossible for the reasons just explained. An appropriate nonlinear transformation "separates" the grid fields from the theta oscillations they are created from, allowing them to serve as an independent basis set from which Gaussian place fields can be successfully constructed.

In simulations presented here, the required nonlinear transformation was achieved by multiplying (rather than linearly summing) paired theta oscillations to produce the grid envelopes [Eq. (15)]. We have conducted simulations to empirically verify that if beat interference patterns are produced by linear summation of theta oscillations instead of multiplication, then the resulting grid fields cannot serve as a basis set for constructing Gaussian place fields in the second stage of our model (data not shown).

SIMULATION RESULTS

In this section, we present simulations with our three-stage network to show that this architecture can reproduce the firing properties of grid cells and place cells. All simulations were conducted on a straight linear track, and assumed a constant running speed of 50 cm/s from left to right on the track.

Phase Precession by Grid Cells

O'Keefe and Burgess (2005) predicted that if the spatially periodic firing patterns of grid cells are derived from beat interference between detuned theta oscillators, then grid cell spikes should undergo phase precession against the theta EEG each time the rat passes through a grid vertex, just as hippocampal place cells undergo phase precession during a rat's passage through their place field. This prediction was confirmed by Hafting et al. (2008), who showed that grid cells in Layer II of entorhinal cortex often exhibit phase precession against the theta EEG; however, Layer III grid cells often tended to show phase-locking with the peak of the theta EEG, rather than phase precession. In simulations with our model, we were able to reproduce both phase precession and phase locking by grid cells, as well as other phase relationships. The manner in which our model produces these phase relationships suggests that different phase precession effects may not be caused by variations in firing properties of grid cells from different layers, but instead by variations in the composition of the EEG signal recorded at different locations.

Figure 4A shows an interference pattern produced by the grid cell $G_{5,0}$ (which receives its unshared input from the theta cell at position $j = 0$ in the fifth theta ring), during a simulation in which the rat traversed a 250-cm straight linear track at a constant speed of 50 cm/s. The dashed horizontal line indicates an arbitrary spike threshold; to measure phase precession, we assumed that the grid cell fired a single action potential at the peak of each carrier cycle that exceeded this threshold (vertical lines).

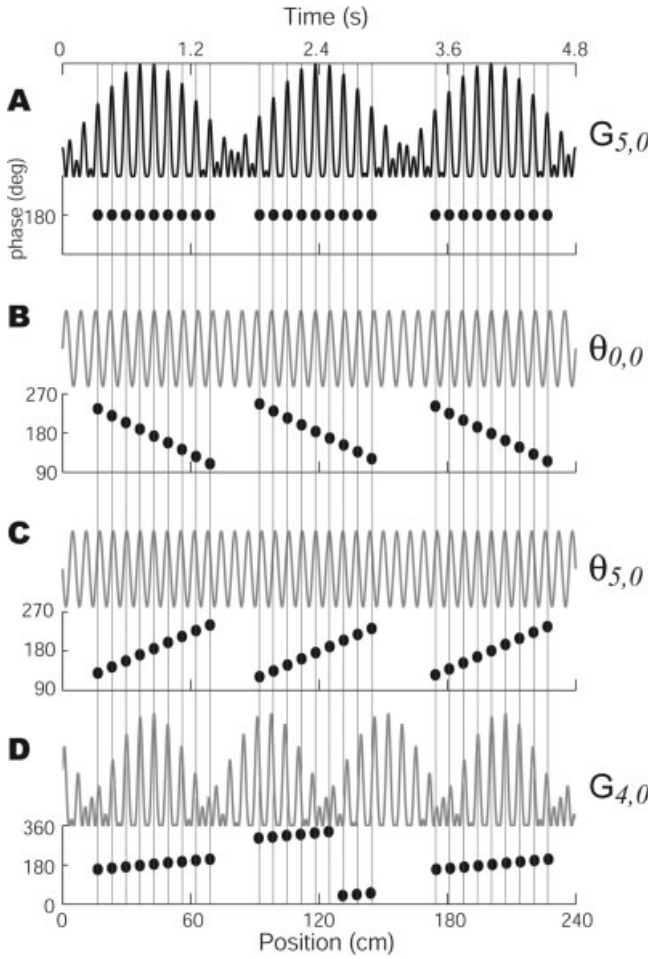

FIGURE 4. Phase precession by grid cells. (A) The interference waveform for grid cell $G_{1,0}$ (top), with the timing of its "spikes" plotted against the phase of its own carrier signal (bottom). (B) The oscillation generated by theta cell $\theta_{0,0}$ (top), with the timing of $G_{1,0}$'s "spikes" plotted against the phase of $\theta_{0,0}$ (bottom). (C) The oscillation generated by theta cell $\theta_{i,j}$ (top), with the timing of $G_{1,0}$'s "spikes" plotted against the phase of $\theta_{i,j}$ (bottom). (D) The interference waveform for grid cell $G_{4,0}$ (top), with the timing of $G_{1,0}$'s "spikes" plotted against the phase of $G_{4,0}$'s carrier signal (bottom).

The scatter plot in Figure 4A (bottom graph) shows the phase of grid cell $G_{5,0}$'s spikes with respect to its own carrier signal. Since the spikes always occur at the peak of their own carrier, and since the carrier peak corresponds to 180° of phase, the spikes exhibit "phase locking" with the peaks of their own carrier at 180°. This result may seem trivial, but such phase locking was reported to occur in Layer III grid cells by Hafting et al. (2008). If neighboring Layer III grid cells receive a shared input from a "reference" oscillator and unshared inputs from neighboring theta cells within the same ring attractor (so that they have identical frequencies and similar phases), then these Layer III cells would exhibit nearly synchronous carriers, which could oscillate coherently and thereby dominate the local theta EEG recorded in Layer III. The result would be phase locking as shown in Figure 4A and reported by Hafting et al. (2008).

Figure 4B shows the output of the reference oscillator theta cell, $\theta_{0,0}$, that projected to all grid cells. The scatter plot in Figure 4B shows the timing of $G_{5,0}$'s suprathreshold carrier peaks against the phase of $\theta_{0,0}$. Here, we see that grid cell $G_{5,0}$'s spikes precess backward through 360° of phase on successive theta cycles as the rat passes through each grid vertex, as observed for Layer II cells by Hafting et al. (2008). This simulation result suggests that as in our model, grid cells in Layer II may share a common input from a single "reference frequency" theta oscillator that has a lower frequency than all other theta oscillators, and this common theta input dominates the hippocampal EEG in Layer II to produce the classical phase precession of grid cell spikes.

Figure 4C shows the output of a velocity-modulated theta cell, $\theta_{5,0}$, which was the source of grid cell $G_{5,0}$'s unique unshared input. The scatter plot shows the timing of $G_{5,0}$'s suprathreshold carrier peaks against the phase of $\theta_{5,0}$. Grid cell $G_{5,0}$'s spikes "pro-cess" (rather than "pre-cess") forward through 360° of phase on successive theta cycles, exactly the opposite of the standard phase precession effect shown in Figure 4B. This type of phase "pro-cession" has not been reported to occur in grid cells, and perhaps this is because as in our model, each individual grid cell receives a different high-frequency theta input. Since the high-frequency theta inputs to each grid cell oscillate at different frequencies and phases, there is little coherence among these high-frequency theta oscillations within the tissue, and they would be poorly detected by EEG electrodes, possibly explaining why forward phase procession is not seen in experiments.

Figure 4D shows an interference pattern produced by the grid cell $G_{4,0}$, which has a different carrier and beat frequency from grid cell $G_{5,0}$ in Figure 4A. The scatter plot in Figure 4D shows the timing of $G_{5,0}$'s suprathreshold carrier peaks against the carrier phase of $G_{4,0}$. Here, we see that grid cell $G_{5,0}$'s spikes are nearly phase locked to $G_{4,0}$'s carrier on each passage through a grid vertex, but the phase at which the locking occurs is different on each vertex traversal. Hence, if the phase of spikes was averaged over many vertex crossings, grid cell $G_{5,0}$'s spikes would show no consistent phase relationship with the $G_{5,0}$ carrier. Some grid cells exhibited such phase inconsistency in the study of Hafting et al. (2008), especially in Layer III. Our model suggests that this may happen when the theta EEG is dominated by carrier frequencies of grid cells other than the one from which spikes are being recorded. If this prediction is correct, then theta cells that show phase inconsistency when spike times are averaged over many vertex crossings might show phase locking at an arbitary phase when spike times are analyzed for single vertex crossings, as in the simulations of Figure 4D.

In summary, the simulations of Figure 4 suggest that differences among grid cells in their phase precession effects may primarily result from differences in the composition of the EEG signal recorded in different layers, and not differences in the functional properties of grid cells themselves. The model predicts that all grid cells should exhibit standard phase precession (Fig. 4B) when their spike times are plotted against the reference oscillation, $\theta_{0,0}$. Therefore, grid cells in Layer III—which rarely showed phase precession the study of Hafting et al. (2008)—might show phase precession more often if their spike times were plotted against the theta EEG recorded from Layer II, where phase precession is more commonly observed.

Spatial Frequency Content of Gaussian Place Fields

In our model, outputs from one-dimensional grid cells were summed to form unidimensional Gaussian place fields on the linear track. The spatial frequency spectrum of a Gaussian depends upon its width [Eq. (18)]. In the rat brain, the sizes of place fields are graded along the septo-temporal axis of the hippocampus, with smaller fields near the septal pole and larger fields near the temporal pole (Jung et al., 1994; Maurer et al., 2005; Kjelstrup et al., 2008). In addition, grid cells decrease their spatial frequencies (and thus increase their vertex spacings) along the dorsoventral axis of the entorhinal cortex (Hafting et al., 2005; Sargolini et al., 2006; Brun et al., 2008).

Figure 5 shows two simulated place fields for a rat running a 10-m straight linear track: a small place field corresponding to a cell in the dorsal hippocampus (blue), and a large place field corresponding to a cell in the ventral hippocampus (red). The small and large place fields were generated by setting the width of the target Gaussians to $\sigma = 5$ cm or $\sigma = 33$ cm, respectively [Eq. (17)]. Figure 5D shows the target Gaussians (left panel), and their corresponding spatial frequency spectra computed from Eq. (18) (right panel). The left side of Figure 5A shows membrane potentials of the dorsal and ventral place cells formed by summing input from all 72 grid cells. Note that the membrane potentials exhibit a high-frequency oscillation corresponding to theta rhythm. To infer place cell "firing," we assumed that spikes were generated when the membrane exceeded a threshold of −60 mV (dashed line), so a cell's place field was defined as the region of the track where its membrane potential exceeded this threshold.

The right side of Figure 5A shows the weight vector solutions that were derived by the pseudoinverse algorithm to produce the place cell membrane potentials shown on the left. To form the dorsal place cell (small firing field), the fitting algorithm attached large weights to grid cells across the entire range

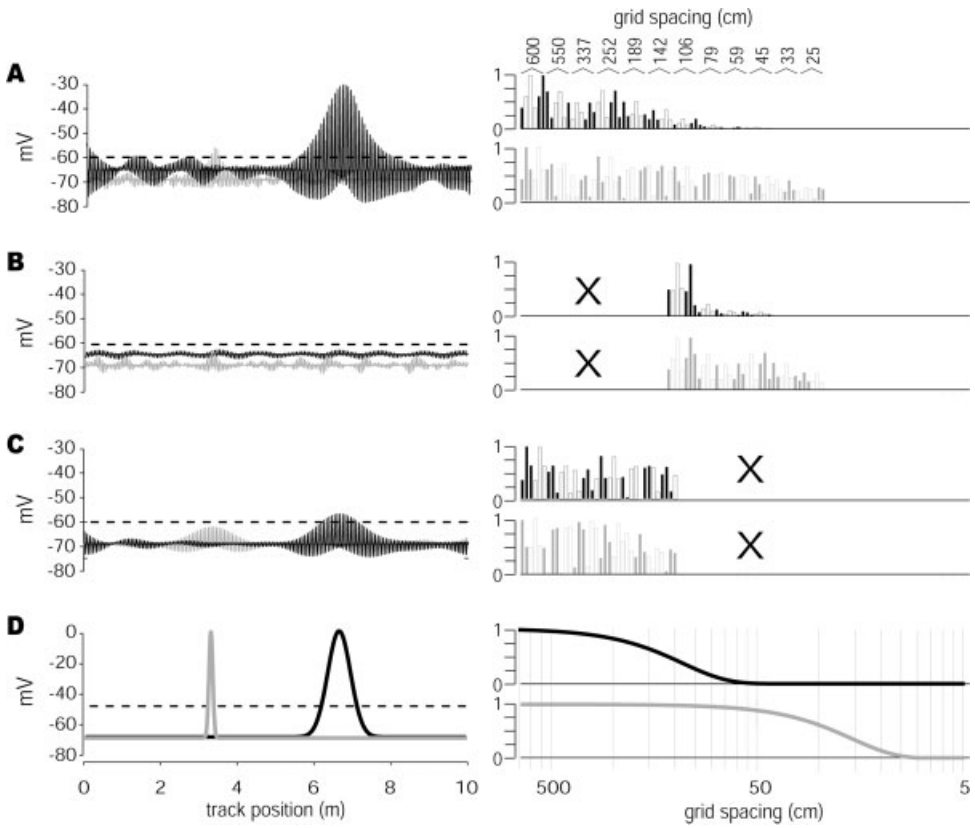

FIGURE 5. Spatial frequency content of Gaussian place fields. Left column shows simulated place cell membrane potentials (*y*-axis) as a rat runs across the length of a 10-m linear track (*x*-axis). Right column shows the absolute value of the normalized weight (*y*-axis) at each spatial frequency (*x*-axis, logarithmic scale) in the Fourier spectra of the Gaussian place fields at left. In the weight vector plots (A–C, right panels), each of the 72 bars represents the weight of one of the 72 grid cells, with filled and empty bars representing positively and negatively weighted inputs, respectively (the DC weight, w_k, is omitted from the plot for scale reasons). (A) Membrane potentials and weight vectors of two simulated place cells with large (black) and small (gray) place fields formed by summing input from all 72 grid cells. (B) Same as "A" except only 36 grid cells with high spatial frequencies were summed. (C) Same as "A" except only 36 grid cells with low spatial frequencies were summed. (D) Target Gaussian place fields for the simulations in "A–C" (left) and their corresponding spatial frequency spectra (right, *x*-axis is plotted on a logarithmic scale).

of grid spacings. This was because the spatial frequency spectrum of the small Gaussian spanned the entire range of spatial frequencies that was contained in the basis set (blue trace, right side of Fig. 5D). But to form the ventral place cell (large firing field), the fitting algorithm only attached large weights to grid cells with low spatial frequencies (i.e., large vertex spacings), because the spatial frequency spectrum of the large Gaussian only covered the low end of the spatial frequencies in the basis set (red trace, right side of Fig. 5D). These simulations show that ventral place cells with large firing fields only need to sum inputs from grid cells with large vertex spacings, but dorsal place cells with small firing fields must sum input from grid cells with both large and small grid spacings.

To further illustrate this, we examined how place fields would look if they were constructed from a subpopulation of grid cells with only small or large vertex spacings. For this, the pseudoinverse algorithm was used to obtain an optimal fit to the Gaussian target using only half of the grid cells in the basis set (i.e., only 36/72 grid cells); however, the DC weighting term w_k was always retained. Figure 5B shows place cell outputs when only grid cells with small vertex spacings were summed; this can be equated with selectively lesioning the ventral entorhinal cortex to destroy large grid fields, while leaving small grid fields intact in the dorsal entorhinal cortex. After this "lesion," the peak membrane potentials of both the large and small place cells fell below spike threshold, so that neither cell exhibited a place field anymore. Some spatial firing might be recovered if the spike threshold were reduced to compensate for this, but since the attenuated peaks are similar in size to the noise background, this would probably cause the place cell to fire at multiple locations on the track. This result is consistent with our formal prediction that all place cells—even dorsal place cells with small firing fields—must receive input from large grids to exhibit unitary firing fields in large environments. The analytically derived frequency spectra in Figure 5D clearly show why this is the case; both large and small place fields contain significant power at low spatial frequencies, so eliminating these frequencies from the basis set is detrimental to the Gaussian fit.

What happens when high (rather than low) spatial frequencies are eliminated from the basis set? This would correspond to lesioning the dorsal rather than ventral entorhinal cortex. Figure 5C shows that when only the 36 grid cells with the largest vertex spacings were summed, the large firing field of the ventral place cell became smaller, because the peak membrane potential was reduced and consequently the spike threshold was exceeded over a smaller region of the track. However, a compensatory reduction in the place cell's spike threshold could restore the place field to nearly its original width. Thus, the spatial tuning of the ventral place cell was well preserved after eliminating the highest spatial frequencies in the basis set. The small firing field of the dorsal place cell was more disrupted, because the field's peak became both smaller and wider. The attenuated peak no longer exceeded the spike threshold at any location on the track, so there was no longer a place field. Once again, a compensatory reduction in the spike threshold might restore the cell's place field, but in this case the field would be considerably broader (i.e., less sharply tuned) than when the full basis set of 72 grid cells was used (Fig. 5A). This is because the sharpness of the small place field's peak is dependent upon from grid fields with high spatial frequencies.

These simulation results suggest that after ventral entorhinal lesions to destroy large grid fields, place cells in both dorsal and ventral hippocampus should no longer fire selectively at a single location in an environment; instead, multiple firing fields may emerge (if the spike threshold were lowered, see Fig. 5B). By contrast, after dorsal entorhinal lesions to destroy small grid fields, place cells in ventral hippocampus may not be affected at all, but dorsal place cells would be likely to exhibit broader tuning of their firing fields (if the spike threshold were lowered, see Fig. 5C). These predictions could be tested experimentally to investigate whether our spatial frequency model provides an accurate description of how place cells are formed from grid cells.

DISCUSSION

Here we have presented a three-stage network model of theta cells, grid cells, and place cells. This model formalizes the computational steps that are necessary for converting a phase-coded position signal stored by theta cells into a rate-coded position signal stored by grid cells and place cells. Previous computational theories have postulated that rate-coded position signals may be stored and updated by an attractor network consisting of a two-dimensional sheet of neurons with planar (Tsodyks and Sejnowski, 1995; Samsonovich and McNaughton, 1997), spherical (Fuhs and Touretzky, 2006), or toroidal (McNaughton et al., 2006) topology. However, all of these theories were founded upon the assumption that the position signal is encoded by the firing rates of place cells or grid cells. The oscillatory interference theory (Burgess et al., 2005, 2007; O'Keefe and Burgess, 2005) suggests that we might discard this assumption, and instead assume that path integration is performed upon a phase-coded position signal stored by theta oscillations. Here we have argued that a useful neural architecture for achieving this is the ring attractor circuit, which has previously been proposed to perform angular path integration in the head-direction system (Skaggs et al., 1995; Redish et al., 1996; Zhang, 1996a,b; Song and Wang, 2005).

Ring Attractor Model of the Velocity-Modulated Theta Oscillator

The basic building block of a circuit for path integration by oscillatory interference is a velocity-modulated oscillator (Burgess, 2008). It has been hypothesized that subthreshold membrane oscillations within grid cells could serve as velocity-modulated theta oscillators (Burgess et al., 2005, 2007; Giocomo et al., 2007; Hasselmo et al., 2007), but here we have proposed an alternative possibility: velocity-modulated theta rhythm may be produced by subcortical ring attractor networks. We have argued that the ring attractor provides a natural architecture for generating frequency-modulated theta oscillations [see Eqs. (10)–(13)]. Each neuron in the ring attractor is a theta cell, which bursts at a frequency determined by which ring it resides in and a phase determined by its position in that ring. If our prediction is correct that velocity-modulated oscillators correspond to individual theta cells, then we might be able to record these cells using extracellular electrodes in freely behaving rats.

Theta-bursting cells are found throughout the hippocampal circuitry, but evidence indicates that the theta rhythm originates within subcortical structures such as the raphe nuclei and mammillary bodies (for review, see Vertes and Kocsis, 1997; Vertes et al., 2001; Pan and McNaughton, 2004; Sharp and Koester, 2008), immediately adjacent to structures where ring attractors for angular path integration by head-direction cells are thought to reside (Blair et al., 1998; Sharp et al., 2001a,b; Basset et al., 2007). These subcortical areas are well positioned to receive ascending input from the vestibular and motor systems, which could encode the velocity signals that must be integrated to generate the position signal. Thus, we hypothesize that these subcortical areas may contain a bank of ring attractors for generating velocity-modulated theta oscillations. We are currently testing this hypothesis by recording theta cells in the raphe nuclei and mammillary bodies of freely behaving rats, to seek evidence for the presence of ring attractors. Our model predicts that if we simultaneously record two theta cells residing in different rings (but not the same ring), then the phase angle between their theta bursts (measurable in cross-correlograms between the two cells) should vary systematically as a function of the rat's position in the environment, thereby reflecting a phase code of the rat's position. In a straight linear track environment, the phase angle between two theta cell burst patterns should vary with a characteristic period along the length of the track, much like our simulated one-dimensional grid cells. In a two-dimensional environment, there would probably be a directional component to the velocity signal that modulates the theta frequencies, as predicted by other models (Burgess et al., 2007; Hasselmo et al., 2007; Burgess, 2008;

Hasselmo, 2008). If so, then the phase angle between a pair of theta cells residing in different rings would trace an oriented sinusoidal grating over the surface of the environment, much like that depicted in Figure 6 of the article by Burgess (2008) elsewhere in this special issue. But the spike train of any individual theta cell would exhibit no spatial tuning whatsoever, a point which is nicely illustrated by path plots of simulated phase-coding neurons in Figure 2C of the article by Hasselmo (2008) elsewhere in this special issue. Like our ring attractor model, the models of Burgess (2008) and Hasselmo (2008) both predict that the rat's position may be encoded by the relative phases of bursts in rhythmic neurons, but as of yet, such a phase-coded position signal has never been experimentally observed. If and when such a signal is discovered, it may become possible to test competing predictions of the ring attractor model vs. these other models concerning the exact nature of the positional phase code.

Topographic Organization of Grid Cells

The ring attractor model of the theta CPG provides a circuit-based framework for "sorting" theta oscillations according to their frequencies and phases; theta cells in different rings oscillate at different frequencies, whereas theta cells within the same ring oscillate at different phases of the same frequency. In the entorhinal cortex, grid cells that are adjacent to one another tend to have similar vertex spacings but differing translational phases (Hafting et al., 2005). In our model, this corresponds to a pair of grid cells that receive their unshared inputs from different theta cells in the same ring attractor. By contrast, grid cells that are far from one another in the entorhinal cortex tend to have different vertex spacings, with smaller spacings encountered in dorsal regions and larger spacings encountered in ventral regions (Hafting et al., 2005; Sargolini et al., 2006; Brun et al., 2008). In our model, "dorsal" and "ventral" grid cells are those that receive their unshared input from theta rings with larger vs. smaller values of the λ_i parameter, respectively (see Fig. 3).

It has been reported that as a recording electrode is advanced along the dorsoventral axis of entorhinal cortex, the characteristic spacing of grid cells increases in discrete increments by an approximately constant multiplicative factor of $\sim$1.7 (Barry et al., 2007). Our model predicts that groups of grid cells receiving input from different ring attractors should have different grid spacings. So possibly, discrete transitions of the grid spacing could correspond to passage of the electrode between regions of tissue that receive input from different ring attractors. Our analysis of the spatial frequency content of Gaussian place fields caused us to set the λ_i parameter of each theta ring in such a way that grid field spacings increased linearly on a logarithmic scale; this is consistent with the observation that grid spacings in entorhinal cortex change in discrete increments by a constant multiplicative (rather than linear) factor.

Our simulations of grid cell phase precession (Fig. 4) propose that compartmentalization of inputs to entorhinal cortex from different ring attractors might affect the composition of the theta EEG signal recorded in different cortical layers. We thus propose that such layer-specific differences in the EEG signal—and not in the firing properties of grid cells themselves—may account for different patterns of phase precession that are observed in different grid cell subpopulations (Hafting et al., 2008).

Spatial Frequency Model of Place Cell Formation

Using linear systems analysis, we have shown that the size of a Gaussian place field determines its spatial frequency spectrum, which in turn defines which grid spacings a place cell must sum inputs from. It has previously been argued that dorsal entorhinal grid cells with small vertex spacings may project to dorsal hippocampus to create place cells with small place fields, and ventral grid cells with large vertex spacings may project to ventral hippocampus to create place cells with large place fields (McNaughton et al., 2006; Solstad et al., 2006; Brun et al., 2008; Kjelstrop et al., 2008). Our simulations suggest that this is only half correct; while it is true that place cells with large firing fields only need to receive input from grid cells with large vertex spacings, we predict that place cells with small unitary firing fields must receive input from grid cells with small as well as large spacings. This is because the spatial frequency spectrum of a small Gaussian bump includes both low and high spatial frequencies (see Fig. 5D). If place cells in the dorsal hippocampus do not receive input from both large and small grid fields, then they should not be able to form small unitary place fields in large environments, as they appear to do (Kjelstrop et al., 2008). These predictions could be tested by recording hippocampal place cells after selective lesions of either dorsal or ventral entorhinal cortex. Our spatial frequency model predicts that after lesions of dorsal entorhinal cortex, ventral hippocampal place cells would be unaffected and dorsal place cells would show enlargement of their small unitary firing fields (Fig. 5C). But after lesions of the ventral entorhinal cortex, all place cells should exhibit a loss of unitary firing fields (and possibly an emergence of multiple fields) in large environments (Fig. 5B).

Two-Dimensional Environments

To formulate our ring attractor and spatial frequency theories as clearly as possible, we have only considered the simplified case of a rat running at constant velocity on a linear track. Our three-layer model can be extended to simulations of open field environments, and prior studies provide clear guidance as to how this can be done in the future. The first and second stages of our model—in which grid cells are formed by oscillatory interference between theta oscillations—are formally equivalent to other models which have demonstrated that two-dimensional grid fields can be formed by oscillatory interference (Burgess et al., 2007; Giocomo et al., 2007; Hasselmo et al., 2007; Giocomo and Hasselmo, 2008). To produce hexagonal grids in the plane, these models assumed that different theta oscillators are modulated by oriented velocity signals that encode the rat's movement speed along different directional vectors. In our ring attractor implementation, this is equivalent to assuming that several independent ring attractors exist for each value of λ_i

(rather than just one, as in Fig. 3), and that each ring's oscillation frequency is modulated by a velocity signal that encodes movement along a different directional vector. Elsewhere in this issue, Burgess (2008) analyzes ways in which the directional velocity signal might be decomposed within the oscillatory interference circuit, showing for example that hexagonal grids can be formed when grid cells receive input from a reference oscillator plus several other velocity-modulated theta oscillators. This analysis can be directly applied to our ring attractor implementation, by assuming that each grid cell in the second stage of our model receives input from the reference oscillator, $\theta_{0,0}$, plus several theta cells in different ring attractors that share the same value of λ_i but are modulated by running speed along differing directional vectors.

The second and third stages of our model—in which place fields are formed by summing a basis set of grid fields through a pseudoinverse-derived weight vector—are formally equivalent to the model of Blair et al. (2007). This model showed that two-dimensional grid fields can serve as a basis set for constructing place fields represented as radial Gaussians (as well as more complex two-dimensional images, such as faces). The spatial frequency model described here can be extended to cover this case by equating the spatial frequency ω [Eq. (18)] with the vertex spacing of the planar grids.

Phase to Rate Code . . . and Back Again?

The network we have described here is a feedforward model for converting a phase-coded into a rate-coded position signal. However, the rat brain may also include circuitry for performing the reverse operation. Oscillatory interference models presuppose that path integration is performed upon the phase-coded position signal, since path integration involves velocity modulation of theta oscillators that store the phase-coded signal. Phase is a continuous (rather than discrete) variable, so the phase-coded position signal is a good substrate for path integration of the rat's continuous movements through space. However, the accumulation of integration errors over time can cause a path-integrated position signal to become inaccurate, and in these circumstances it may be desirable to discontinuously "reset" the integrator (Skaggs et al., 1995; Touretzky and Redish, 1996; Samsonovich and McNaughton, 1997). This resetting operation might best be performed upon the rate-coded rather than phase-coded position signal, because the corrected position could be encoded as a pattern of activity among place cells and grid cells that is associated with familiar cues at the location where the position update occurs. Burgess et al. (2007) and Burgess (2008) have hypothesized that place cells might play a role in realigning the spatial phases of entorhinal grid cells to reset the path integrator. If so, then our model implies that this realignment signal must also propagate backward to reset the temporal phases of the subcortical ring oscillators. Anatomical connections that might achieve this are found within the descending limb of the classical Papez (1937) circuit, along which limbic cortical areas send projections to the mammillary regions where we propose that the subcortical ring attractors may be located.

Acknowledgments

The authors thank Adam Welday and two anonymous reviewers for helpful comments.

REFERENCES

Acker CD, Kopell N, White JA. 2003. Synchronization of strongly coupled excitatory neurons: Relating network behavior to biophysics. J Comput Neurosci 15:71–90.

Barry C, Hayman R, Burgess N, Jeffery KJ. 2007. Experience-dependent rescaling of entorhinal grid cells. Nat Neurosci 10:682–684.

Basset JP, Tullman ML, Taube JS. 2007. Lesions of the tegmentomammillary circuit in the head direction system disrupt the head direction signal in the anterior thalamus. J Neurosci 27:7564–7577.

Blair HT, Cho J, Sharp PE. 1998. Role of the lateral mammillary nucleus in the rat head-direction circuit: A combined single-unit recording and lesion study. Neuron 21:1387–1397.

Blair HT, Welday AW, Zhang K. 2007. Scale-invariant memory representations emerge from moiré interference between grid fields that produce theta oscillations: A computational model. J Neurosci 27: 3211–3229.

Brun VH, Solstad T, Kjelstrup KB, Fyhn M, Witter MP, Moser EI, Moser M-B. 2008. Progressive increase in grid scale from dorsal to ventral medial entorhinal cortex. Hippocampus 18:1200–1212.

Burgess N. 2008. Grid cells and theta as oscillatory interference: Theory and predictions. Hippocampus 18:1157–1174.

Burgess N, Barry C, Jefferies KJ, O'Keefe J. 2005. A grid and place cell model of path integration utilizing phase precession versus theta. 1st Annual conference on Computational Cognitive Neuroscience, Washington, DC.

Burgess N, Barry C, O'Keefe J. 2007. An oscillatory interference model of grid cell firing. Hippocampus 17:801–812.

Buzsaki G. 2002. Theta oscillations in the hippocampus. Neuron 33:325–340.

Egorov AV, Hamam BN, Fransen E, Hasselmo ME, Alonso AA. 2002. Graded persistent activity in entorhinal cortex neurons. Nature 420:173–178.

Fiete IR, Burak Y, Brookings T. 2008. What grid cells convey about rat location. J Neurosci 28:6858–6871.

Fuhs MC, Touretzky DS. 2006. A spin glass model of path integration in rat medial entorhinal cortex. J Neurosci 26:4266–4276.

Giocomo LM, Hasselmo ME. 2008. Computation by oscillations: Implications of experimental data for theoretical models of grid cells. Hippocampus 18:1186–1199.

Giocomo LM, Zilli EA, Fransen E, Hasselmo ME. 2007. Temporal frequency of subthreshold oscillations scales with entorhinal grid field spacing. Science 315:1719–1722.

Hafting T, Fyhn M, Molden S, Moser MB, Moser EI. 2005. Microstructure of a spatial map in the entorhinal cortex. Nature 436:801–806.

Hafting T, Fyhn M, Bonnevie T, Moser MB, Moser EI. 2008. Hippocampus-independent phase precession in entorhinal grid cells. Nature 453:1248–1252.

Hasselmo ME. 2008. Grid cell mechanisms and function: Contributions of entorhinal persistent spiking and phase resetting. Hippocampus 18:1213–1229.

Hasselmo ME, Giocomo LA, Zilli EA. 2007. Grid cell firing may arise from interference of theta frequency membrane potential oscillations in single neurons. Hippocampus 17:1252–1271.

Hayman R, Jeffery KJ. 2008. Generating hippocampal place fields from entorhinal grids. Hippocampus 18.

Jung MW, Wiener SI, McNaughton BL. 1994. Comparison of spatial firing characteristics of units in dorsal and ventral hippocampus of the rat. J Neurosci 14:7347–7356.

Kjelstrup KB, Solstad T, Brun VH, Hafting T, Leutgeb S, Witter MP, Moser EI, Moser MB. 2008. Finite scale of spatial representation in the hippocampus. Science 321:140–143.

Lengyel M, Szatmary Z, Erdi P. 2003. Dynamically detuned oscillations account for the coupled rate and temporal code of place cell firing. Hippocampus 13:700–714.

Maurer AP, Vanrhoads SR, Sutherland GR, Lipa P, McNaughton BL. 2005. Self-motion and the origin of differential spatial scaling along the septo-temporal axis of the hippocampus. Hippocampus 15:841–852.

McNaughton BL, Battaglia FP, Jensen O, Moser EI, Moser MB. 2006. Path integration and the neural basis of the 'cognitive map'. Nat Rev Neurosci 7:663–678.

Molter C, Yamaguchi Y. 2008. Impact of temporal coding of presynaptic entorhinal cortex grid cells on the formation of hippocampal place fields. Neural Netw 21:303–310.

Moser EI, Moser M-B. 2008. A metric for space. Hippocampus 18.

O'Keefe J, Burgess N. 2005. Dual phase and rate coding in hippocampal place cells: Theoretical significance and relationship to entorhinal grid cells. Hippocampus 15:853–866.

O'Keefe J, Dostrovsky J. 1971. The hippocampus as a spatial map. Preliminary evidence from unit activity in the freely-moving rat. Brain Res 34:171–175.

O'Keefe J, Nadel L. 1978. The Hippocampus As a Cognitive Map. Oxford: Oxford University Press.

O'Keefe J, Recce MR. 1993. Phase relationship between hippocampal place units and the EEG theta rhythm. Hippocampus 3:317–330.

Pan WX, McNaughton N. 2004. The supramammillary area: It's organization, functions, and relationship to the hippocampus. Prog Neurobiol 74:127–166.

Papez JW. 1937. A proposed mechanism of emotion. J Neuropsychiatry Clin Neurosci 7:103–112.

Redish AD, Touretzky DS. 1997. Cognitive maps beyond the hippocampus. Hippocampus 7:15–35.

Redish AD, Elga AN, Touretzky DS. 1996. A coupled attractor model of the rodent head-direction system. Network 7:671–685.

Rolls ET, Stringer SM, Eliot T. 2006. Entorhinal cortex grid cells can map to hippocampal place cells by competitive learning. Network 17:447–465.

Samsonovich A, McNaughton B. 1997. Path integration and cognitive mapping in a continuous attractor neural network model. J Neurosci 17:5900–5920.

Sargolini F, Fyhn M, Hafting T, McNaughton BL, Witter MP, Moser MB, Moser EI. 2006. Conjunctive representation of position, direction, and velocity in entorhinal cortex. Science 312: 758–762.

Sharp PE, Blair HT, Cho J. 2001a. The anatomical and computational basis of the rat head-direction cell signal. Trends Neurosci 24:289–294.

Sharp PE, Koester K. 2008. Lesions of the mammillary body region alter hippocampal movement signals and theta frequency: Implications for path integration models. Hippocampus 18:862–878.

Sharp PE, Tinkelman A, Cho J. 2001b. Angular velocity and head direction signals recorded from the dorsal tegmental nucleus of gudden in the rat: Implications for path integration in the head direction cell circuit. Behav Neurosci 115:571–588.

Skaggs WE, Knierim JJ, Kudrimoti HS, McNaughton BL. 1995. A model of the neural basis of the rat's sense of direction. In: Tesauro G, Touretzky D, Leen T, editors. Advances in Neural Information Processing Systems 7. Cambridge, Massachusetts: MIT. pp. 173–180.

Solstad T, Moser EI, Einevoll GT. 2006. From grid cells to place cells: A mathematical model. Hippocampus 16:1026–1031.

Song P, Wang XJ. 2005. Angular path integration by moving "hill of activity": A spiking neuron model without recurrent excitation of the head-direction system. J Neurosci 25:1002–1014.

Taube JS, Muller RU, Ranck JB Jr. 1990. Head-direction cells recorded from the postsubiculum in freely moving rats. I. Description and quantitative analysis J Neurosci 10:420.

Tolman EC. 1948. Cognitive maps in rats and man. Psychol Rev 55:189–208.

Touretzky DS, Redish AD. 1996. Theory of rodent navigation based on interacting representations of space. Hippocampus 6:247–270.

Tsodyks MV, Sejnowski TJ. 1995. Associative memory and hippocampal place cells. Int J Neural Syst 6:81–86.

Vanderwolf CH. 1969. Hippocampal electrical activity and voluntary movement in the rat. Electroencephalogr Clin Neurophysiol 26:407–418.

Vertes RP, Kocsis B. 1997. Brainstem-diencephalo-septohippocampal systems controlling the theta rhythm of the hippocampus. Neuroscience 81:893–926.

Vertes RP, Albo Z, Viana Di Prisco G. 2001. Theta-rhythmically firing neurons in the anterior thalamus: Implications for mnemonic functions of Papez's circuit. Neuroscience 104:619–625.

Xie X, Hahnloser RHR, Seung HS. 2002. Double-ring network model of the head-direction system. Phys Rev E 66:041902.

Zhang K. 1996a. Representation of spatial orientation by the intrinsic dynamics of the head direction cell ensemble: A theory. J Neurosci 16:2112.

Zhang K. 1996b. Representing head direction by attractor dynamics and the dynamic shift mechanisms. In: Bower JM, editor. Computational Neuroscience: Trends in Research. San Diego: Academic Press. pp 415–420.